1912–1926 *Nucleic Acids Research, 2018, Vol. 46, No. 4* *Published online 5 January 2018*
doi: 10.1093/nar/gkx1312

Interplay between RNASEH2 and MOV10 controls LINE-1 retrotransposition

Jongsu Choi[1,2], Sung-Yeon Hwang[1,2] and Kwangseog Ahn[1,2,*]

[1]Center for RNA Research, Institute for Basic Science, Seoul 08826, Republic of Korea and [2]School of Biological Sciences, Seoul National University, Seoul 08826, Republic of Korea

Received September 28, 2017; Revised December 20, 2017; Editorial Decision December 21, 2017; Accepted December 23, 2017

ABSTRACT

Long interspersed nuclear element 1 is an autonomous non-long terminal repeat retrotransposon that comprises ∼17% of the human genome. Its spontaneous retrotransposition and the accumulation of heritable L1 insertions can potentially result in genome instability and sporadic disorders. Moloney leukemia virus 10 homolog (MOV10), a putative RNA helicase, has been implicated in inhibiting L1 replication, although its underlying mechanism of action remains obscure. Moreover, the physiological relevance of MOV10-mediated L1 regulation in human disease has not yet been examined. Using a proteomic approach, we identified RNASEH2 as a binding partner of MOV10. We show that MOV10 interacts with RNASEH2, and their interplay is crucial for restricting L1 retrotransposition. RNASEH2 and MOV10 co-localize in the nucleus, and RNASEH2 binds to L1 RNAs in a MOV10-dependent manner. Small hairpin RNA-mediated depletion of either RNASEH2A or MOV10 results in an accumulation of L1-specific RNA-DNA hybrids, suggesting they contribute to prevent formation of vital L1 heteroduplexes during retrotransposition. Furthermore, we show that RNASEH2-MOV10-mediated L1 restriction downregulates expression of the rheumatoid arthritis-associated inflammatory cytokines and matrix-degrading proteinases in synovial cells, implicating a potential causal relationship between them and disease development in terms of disease predisposition.

INTRODUCTION

Long interspersed nuclear element 1 (LINE-1; L1), the only active non-long terminal repeat (LTR) transposable element in humans, comprises ∼17% of the whole human genome (1). L1 retrotransposition is primarily known to be active in germline cells or embryonic stem cells during early embryonic development, but the L1 mobility in somatic and transformed human cells is still controversial. L1 is capable of retrotransposing autonomously across the genome through target site-primed reverse transcription (TPRT) in an L1 ORF2p-dependent manner (2,3). L1 retrotransposition has long been considered to be a causative factor of genomic instability and diverse genetic alterations throughout the entire human genome (4). The accumulation of heritable L1 insertions can cause the evolvability of human genetic disorders (5,6). Furthermore, it has been suggested that L1-derived nucleic acids have the potential to stimulate a range of aberrant inflammatory responses, including autoimmune responses. Mutations of genes that contribute to cellular nucleic acid metabolism appear to be linked to immunological abnormalities (7,8); however, it is less clear how the L1-derived nucleic acids trigger aberrant immune responses and early onset of certain autoimmune diseases.

Moloney leukemia virus 10 homolog (MOV10), a member of the ATP-dependent RNA helicase superfamily 1, was first identified as a factor that prevents production of infectious Moloney leukemia virus (MLV) in mice (9). MOV10 displays broad RNA binding properties and 5′ to 3′ RNA-duplex unwinding activity (10). Interestingly, MOV10 also inhibits replication of a number of retroviruses (11,12) and mobility of retroelements, including LTR and non-LTR retrotransposons in somatic cells (13–17). Considering phylogenetic studies (18,19), non-LTR retrotransposons are regarded as likely progenitors of either retroviruses or endogenous retroelements. Accordingly, it is not surprising that MOV10 is capable of inhibiting L1 retrotransposition.

MOV10 is associated with the Argonaute 2 protein (AGO2) of the RNA-induced silencing complex that is required for miRNA-mediated gene silencing (20); however, MOV10-mediated L1 restriction occurs independent of this pathway (15). Furthermore, MOV10 co-localizes with L1 ORF1p in cytoplasmic processing bodies (P-bodies) (11,21) that play a role in the storage and degradation of translationally repressed mRNAs. Therefore, MOV10 has been implicated in facilitating sequestration of L1 ribonucleoproteins (RNPs) and a degradation of L1 RNAs (15). On the other hand, several studies have highlighted diverse functions of nuclear MOV10 (22), including suppression

*To whom correspondence should be addressed. Tel: +82 2 880 9233; Email: ksahn@snu.ac.kr

of retroelements (17). Hence, the exact mode of MOV10-mediated L1 restriction remains uncertain.

Ribonuclease H2 (RNASEH2) is a nuclear heterotrimeric enzyme that hydrolyzes RNA strands of RNA-DNA hybrids, which spontaneously form during cellular transcription and DNA replication (23,24). Unlike RNASEH1, RNASEH2 is capable of removing the 5′-phosphodiester bond of ribonucleotides (rNTPs) embedded in DNA duplexes (25). Given that misincorporated ribonucleotides may be the most abundant non-canonical nucleotides present in genomic DNA, their removal by RNASEH2 is likely critical for maintaining genomic integrity (26). RNASEH2 has also been shown to be contributed to human immunodeficiency virus type 1 (HIV-1) replication (27). Due in part to the scarcity of cellular deoxyribonucleoside triphosphates (dNTPs) in terminally differentiated macrophages (28), the HIV-1 reverse transcriptase may misincorporate ribonucleoside triphosphates (rNTPs) into viral cDNA during HIV-1 reverse transcription. For this reason, RNASEH2 has been considered as a positive regulator of HIV-1 replication by eliminating misincorporated rNTPs during HIV-1 reverse transcription (29).

Genetic alterations in any of the three subunits of the human RNASEH2 cause Aicardi-Goutières syndrome (30), an autoimmune encephalopathy with similarities to congenital viral infections (31). A recent study has shown that DNA-RNA immunoprecipitation (DRIP) peaks are enriched in L1 and LTR-containing sequences in RNASEH2-deficient AGS fibroblasts (32). In line with this, homozygotic mutations near the catalytic core of RNASEH2A subunit also result in a substantial decrease in enzymatic activity in mice, thereby upregulating diverse interferon-stimulated genes and increasing L1-derived DNA levels as seen in AGS patients (33). However, it remains unclear whether the increase in L1 DNA is a result of L1 reactivation in either AGS fibroblasts or the mice. Although it has been most recently reported that CRISPR/Cas9-mediated knockout of *RNASEH2A* leads to a substantially reduced retrotransposition (34), the role of RNASEH2 in L1 metabolism is thus far not fully proven.

Herein we report that RNASEH2 contributes to MOV10-mediated L1 inhibition. RNASEH2 interacts with MOV10 in an RNA-dependent manner, and their interplay is essential for suppressing L1 mobility. Further biochemical and microscopic analyses reveal that RNASEH2 associates with L1 RNAs in a MOV10-dependent manner, and that L1-derived RNA-DNA hybrids preferentially accumulate in either RNASEH2A- or MOV10-deficient cells. These findings suggest that RNASEH2 and MOV10 are capable of inhibiting formation of L1-derived RNA-DNA hybrids during L1 retrotransposition. Furthermore, we show that RNASEH2-MOV10-mediated L1 regulation limits induction of inflammatory cytokines and activation of matrix metalloproteinase 3 (MMP-3) in synovial cells, suggesting that L1 regulation potentially affects rheumatoid arthritis-related pathophysiology.

MATERIALS AND METHODS

Plasmids

FLAG-haemagglutinin (HA)-tagged Moloney leukemia virus 10 homolog (F/H-MOV10) was purchased from Addgene (plasmid #10976) (35). HA-MOV10^{K530A} and RNASEH2A^{G37S}-FLAG variants were prepared using site-directed mutagenesis. Substitutions were confirmed by DNA sequencing. L1-*neo*^{TET} (36) was a gift from Dr. Astrid Roy-Engel (Addgene plasmid #51284). L1-luciferase plasmids (pYX015, pYX017) (37) and pAD3TE1 (38) carrying 24 copies of the MS2 stem-loop RNA-binding repeat upstream of the *mneoI* indicator cassette were generously provided by Dr. Wenfeng An and Dr. Aurélien Doucet, respectively. pMS2-GFP was provided by Dr. Robert Singer and purchased through Addgene (plasmid #27121) (39). To generate L1 ORF1p-EGFP construct, we employed the Gateway™ cloning system (Invitrogen). L1 ORF1 was amplified by polymerase chain reaction (PCR) from L1-*neo*^{TET} and cloned into pEGFP-N3 expression vector. For RNA-DNA hybrid-binding retention assay, a fusion protein of the 52-residue RNA-DNA hybrid-binding domain (HB) of RNASEH1 and enhanced green fluorescent protein (EGFP) (hereafter referred to as HB-GFP) was constructed, as previously described (40). The HB domain of RNASEH1 was amplified by PCR and cloned into pEGFP-N3 expression vector.

Cells

HeLa, HEK 293T and SW982 cells were maintained in Dulbecco's modified Eagle's medium (DMEM, Hyclone) supplemented with 10% (v/v) fetal bovine serum (FBS, HyClone), antibiotics mixture (100 units/ml, penicillin-streptomycin, Gibco) and 1% (v/v) GlutaMAX-I (Gibco). Cells were incubated at 37°C under a 5% CO_2 atmosphere.

LINE-1 (L1) retrotransposition assay

For *neo*^{r} expression cassette-based L1 retrotransposition assays, either HeLa or SW982 cells (3×10^5 cells/ml) were transfected with 0.2 ∼ 1 μg of L1-*neo*^{TET} using Lipofectamine™ 3000 (Invitrogen) following the manufacturer's instructions. If indicated, the L1 cassette was co-transfected with either MOV10 or RNASEH2 components (A, B and C) at a ratio of 1:1. After 48 h of incubation, the cells were trypsinized and re-seeded in 60 mm petri-dishes at 2 ∼ 6×10^4 cells/ml, as indicated. Cells were maintained in the presence of G418 (1 mg/ml) for up to 14 days. Subsequently, cells were fixed and stained with 20% ethanol-containing crystal violet solution (Sigma-Aldrich). Colonies were counted manually or digitally using the OpenCFU software (41) with customized micros.

For dual luciferase-mediated retrotransposition assays, HeLa cells (5×10^4 cells/ml) were transfected using Lipofectamine™ 3000 following the manufacturer's instructions. Cells were co-transfected at a 1:1 ratio with the L1-*luc* expression cassette (pYX017) and either MOV10 variants or RNASEH2 components. As a negative control for the assay, pYX015 (an inactive L1-*luc* construct which contains loss-of-function mutations in ORF1p) was trans-

fected, if indicated. Puromycin (Sigma-Aldrich) was added after 24 h of incubation at a final concentration of 1 μg/ml. Cells were harvested at 4 days post-transfection, and luminescence was monitored using the Dual-Luciferase® Reporter Assay System (Promega) following the manufacturer's instructions. L1 activity was determined as the ratio of firefly to *Renilla* luciferase activity (Fluc/Rluc), as previously reported (37). If indicated, the nucleoside reverse transcriptase inhibitor (NRTI), 2′-3′-didehydro-2′-3′-dideoxythymidine (d4T; Stavudine), was added to a final concentration of 50 μM. Typically, cells were treated with complete medium for 24 h prior to transfection, and medium was replaced every 24 ∼ 48 h onward until the endpoint of each experiment.

Quantitative real-time PCR (qPCR)

Equivalent amounts of purified genomic DNA (50 ∼ 100 ng) from each sample were analyzed by qPCR. For RT (reverse transcription)-qPCR, 1 ∼ 2 μg of RNA was reverse-transcribed using the ReverTra Ace qPCR RT Kit (TOYOBO) following the manufacturer's instructions. The resulting complementary DNA (cDNA) was diluted with sterile deionized H_2O (1:10). RT-qPCR reactions were performed in TOPreal qPCR PreMIX (Enzynomics) with 4 μl of the diluted cDNA. The total reaction volume was 20 μl, and all reactions were performed in triplicate. The PCR reactions were performed using the iCycler iQ real-time PCR detection system (Bio-Rad). Data were normalized according to the expression levels of *GAPDH*, *MDM2* and *RN7SL1*, as indicated. Spliced L1 insertions or RNAs were detected with primers specific to an exon-exon junction within the firefly luciferase gene (*Fluc*). qPCR analyses were performed using the following primer sets specific to: spliced *Fluc* (Forward, 5′-CCTTCGTGACTTCCCATTTGCC-3′; Reverse, 5′-GGATGATCTGGTTGCCGAAG-3′), *RNASEH1* (Forward, 5′-AGTTTGCCACAGAGGATGAG-3′; Reverse, 5′- CGCTTGCTGGCTTTCGCCTCCGAT-3′), *THOC1* (Forward, 5′-CAGAGACAAGGGAACACATG-3′; Reverse, 5′-CAGAAGGAGGCGGTAATTCC-3′), *SETX* (Forward, 5′-CTTCATCCTCGGACATTTGAG-3′; Reverse, 5′- TTAATAATGGCACCACGCTTC-3′), *RN7SL1* (Forward, 5′-GGGCTGTAGTGCGCTATGC-3′; Reverse, 5′-CCCGGGAGGTCACCATATT-3′), *GAPDH* (Forward, 5′-GCAAATTCCATGGCACCGT -3′; Reverse, 5′-TCGCCCCACTTGATTTTGG-3′), and *MDM2* (Forward, 5′-GGTTGACTCAGCTTTTCCTCTTG -3′; Reverse, 5′-GGAAAATGCATGGTTTAAATAGCC-3′).

RNA immunoprecipitation (RIP)

RIP was performed to analyze potential interactions between L1 RNAs and associated proteins. Cells were co-transfected with pYX017 (L1-*luc*) and corresponding expression constructs at a 1:1 ratio using Lipofectamine™ 3000 following to manufacturer's instructions. Transfected cells were cross-linked with 1% (v/v) formaldehyde in 1× phosphate-buffered saline (PBS) for 10 min at room temperature, and the reaction was quenched by the addition of 1 M glycine pH 7.0 to a final concentration of 0.25 M and incubated at room temperature for 5 min. Cells were rinsed with ice-cold 1× PBS and resuspended in RIPA buffer (50 mM Tris-HCl pH 7.5, 1% NP-40, 0.5% sodium deoxycholate, 0.05% sodium dodecyl sulphate (SDS), 1 mM ethylenediaminetetraacetic acid (EDTA), 150 mM NaCl, 1 mM dithiothreitol (DTT)) containing 1× cOmplete™ Protease Inhibitor Cocktail (Roche) and RNase inhibitor (Enzynomics). Cell extracts were sonicated and centrifuged for 10 min at 9000 × *g* at 4°C, and the resulting supernatant was pre-cleared by subsequent incubation with Protein G Sepharose (GE healthcare) at 4°C for 1 h. The pre-cleared supernatant was incubated with either anti-HA (Sigma-Aldrich) or anti-FLAG-conjugated agarose beads (Sigma-Aldrich) overnight at 4°C. The beads were then washed with RIPA buffer (50 mM Tris-HCl pH 7.5, 1% NP-40, 1% sodium deoxycholate, 0.1% SDS, 1 mM EDTA, 1 M NaCl, 2 M urea) containing 1× cOmplete™ Protease Inhibitor Cocktail. The beads were resuspended in reverse cross-link buffer (50 mM Tris-HCl pH 7.0, 5 mM EDTA, 10 mM DTT, 1% SDS) and then incubated for 1 h at 70°C. The resulting immunoprecipitated RNAs were isolated with TRIzol™ reagent (Ambion) following the manufacturer's protocol and subjected to RT-qPCR using primers specific to spliced *Fluc* cassette. The IP signal was calculated as enrichment over input using the following equation: $\Delta C_t = 2^{(CtInput - CtIP)}$. The RNA enrichment results were normalized to the results obtained using a control primer pair specific to *RN7SL1* and quantitated using the equation, $\Delta\Delta C_t = \Delta C_t^{experiment} / \Delta C_t^{control}$. Student's *t*-test was used to assess statistical significance.

RNA-DNA hybrid immunoprecipitation (DRIP)

DRIP was performed as described previously (42) with the following modifications. Briefly, corresponding HeLa cells were lysed with lysis buffer (10 mM Tris-HCl pH 8.0, 100 mM NaCl, 25 mM EDTA pH 8.0, 0.5% SDS, 10 μg/ml Proteinase K (MACHEREY-NAGEL)) and incubated overnight at 55°C. If indicated, HeLa cells were transfected with pYX017 (L1-*luc*) using Lipofectamine™ 3000 following to the manufacturer's instructions and harvested at 24 h or 36 h post-transfection. Total nucleic acids were extracted using the standard phenol-chloroform extraction method and resuspended in Tris-EDTA (TE) pH 8.0 (Ambion). The nucleic acids were digested with a restriction enzyme cocktail (20 units of EcoRI, BamHI, HindIII, BsrBI and XhoI; New England BioLabs) overnight at 37°C. The digested nucleic acids were subsequently used for qPCR reactions. As a negative control, half of the sample was treated with 10 units of RNase H (M0297; New England BioLabs) overnight at 37°C. The resulting fragmented DNA samples were isolated using the phenol-chloroform extraction method and resuspended in TE buffer. RNA-DNA hybrids were immunoprecipitated from total nucleic acids by adding 10 μg of S9.6 antibody (ENH001; Kerafast) in IP buffer (10 mM $NaPO_4$ pH 7.0, 140 mM NaCl, 0.05% Triton X-100) and incubating overnight at 4°C. Dynabeads Protein A (50 μl; Invitrogen) were used to pull-down the DNA-antibody complexes. The beads were incubated with the samples at room temperature for 3 h and then washed three times with IP buffer. The DNA was eluted with IP buffer and treated

for 1 h with 10 μl of proteinase K (10 μg/ml) at 55°C. Additionally, RNase A (EN0531; Thermo Fisher Scientific) was added and incubated with the samples for 1 h at 37°C to degrade RNA. Subsequently, DNA was purified following the phenol-chloroform extract method. For DRIP-RT-qPCR, the precipitated nucleic acids were denatured at 98°C and then treated with DNase I (2270B, Takara) at 37°C for 1 h. The resulting RNA was isolated using TRIzol™ reagent. The relative abundances of immunoprecipitated RNA-DNA hybrids at the indicated region were calculated as follows: $\Delta C_t = 2^{(Ct Input - Ct IP)}$. Nucleic acid enrichment was further normalized to a control primer pair specific to either *MDM2* or *RN7SL1* and calculated using the equation, $\Delta\Delta C_t = \Delta C_t^{experiment}/\Delta C_t^{control}$. Student's *t*-test was used to assess statistical significances.

Enzyme-linked immunosorbent assay (ELISA)

SW982 cells (3×10^5 cells/ml) were co-transfected with 0.5 μg of L1-*neo*^{TET} and either MOV10 or RNASEH2 components (A, B and C, respectively) at a ratio of 1:1 using Lipofectamine™ 3000 following the manufacturer's instructions. After incubation for 72 h, the cell culture supernatant was harvested and analyzed by ELISA to detect levels of human IL-6 and TNF-α following the manufacturer's instructions (Human ELISA MAX™, Biolegend).

Matrix metalloproteinase 3 (MMP-3) activity assay

SW982 cells (3×10^5 cells/ml) were co-transfected with 0.5 μg of L1-*neo*^{TET} expression cassette and corresponding components at a ratio of 1:1 using Lipofectamine™ 3000 according to the manufacturer's recommendation. At 72 h post-transfection, the cell culture supernatant was harvested and was analyzed for MMP-3 activity using a fluorescence-based assay following manufacturer's instructions (MMP-3 Activity Assay Kit, Abcam).

Statistical analysis

Statistical analyses were performed using GraphPad Prism 5 (GraphPad Software). Comparisons between two groups were performed using two-tailed Student's *t*-test. Results are expressed as the mean ± SD, and *p*-values < 0.05 are considered statistically significant.

RESULTS

Identification of RNASEH2 as a MOV10-interacting factor

Considering the functions of MOV10 as a putative RNA helicase and an L1 restriction factor, we hypothesized that a novel effector molecule involved in RNA metabolism may be required for MOV10-mediated L1 restriction. To identify proteins that associate with MOV10 during L1 regulation, we co-purified MOV10-interacting proteins using dual-tag affinity purification followed by LC-MS analysis. Of note, we identified the RNASEH2A and B peptides among the prominent bands at ∼43 kDa (Supplementary Table S1 and Figure S1A). Thus, we hypothesized that RNASEH2 functions as an effector molecule in MOV10-mediated L1 restriction.

To assess whether co-purified RNASEH2 is a *bona fide* interacting protein with MOV10, MOV10 expression construct was co-transfected with RNASEH2A, B or C to HeLa cells. As shown in Figure 1A, RNASEH2A, a catalytic core component of RNASEH2, was reproducibly co-immunoprecipitated with MOV10 in whole cell lysates of transfected cells. The two auxiliary subunits of RNASEH2 (B and C) were also co-purified with ectopically expressed MOV10 (Figure 1A). However, their interaction was substantially reduced by treatment with RNase A prior to the immunoprecipitation procedure, suggesting that these protein-protein interactions might be dependent on RNA binding (Figure 1A). Endogenous RNASEH2A was also consistently associated with endogenous MOV10 (Figure 1B), indicating that the co-immunoprecipitation data strongly supported the LC-MS results.

To verify if RNASEH2 functionally interacts with MOV10, we performed a nuclear/cytoplasmic fractionation experiment using HeLa cells. A higher proportion of endogenous MOV10 was found in the cytoplasm than in the nucleus. However, endogenous RNASEH2A was predominantly found in the nucleus (Figure 1C), suggesting a functional association between RNASEH2 and MOV10 in the nucleus.

Because MOV10 interacts with L1 ORF1p (15,43–44) (Supplementary Figure S1B), we next tested whether MOV10 functions as a molecular platform to influence an interaction between RNASEH2 and L1 ORF1p. Small hairpin RNA (shRNA)-mediated depletion of endogenous MOV10 (Figure 1D) markedly decreased the association of RNASEH2 components with L1 ORF1p, suggesting that MOV10 mediates the interaction between RNASEH2 and L1 ORF1p (Figure 1E). Collectively, MOV10 interacts with RNASEH2, and it is required for the association between RNASEH2 and L1 ORF1p.

Interplay between RNASEH2 and MOV10 is required for inhibition of L1 mobility

Since MOV10 controls L1 mobility through its helicase activity (15), we next investigated whether co-purified RNASEH2 would affect the MOV10-mediated L1 restriction. As a proof-of-principle, we performed a cell-based engineered L1-retrotransposition assay (3,36). The expression cassette carried a neomycin phosphotransferase gene (*neo*^{r}) within the 3′ untranslated region (UTR) in an anti-sense orientation relative to a CMV promoter. This gene was disrupted by the addition of intronic sequences. When L1 has been successfully retrotransposed following transcription, self-splicing, TPRT and integration across the genome, the cells become resistant to neomycin (Figure 2A).

Upon ectopic expression of MOV10, the number of G418-resistant colonies was markedly reduced by 4-fold when compared to the control condition (cells transfected with empty vector) (Figure 2B). Consistent with this, transient overexpression of either RNASEH2 or RNASEH2 in combination with MOV10 also effectively impaired L1 mobility to similar level (Figure 2B). These results demonstrated that both RNASEH2 and MOV10 potently suppress L1 mobility and thereby function as negative regulators of L1 retrotransposition.

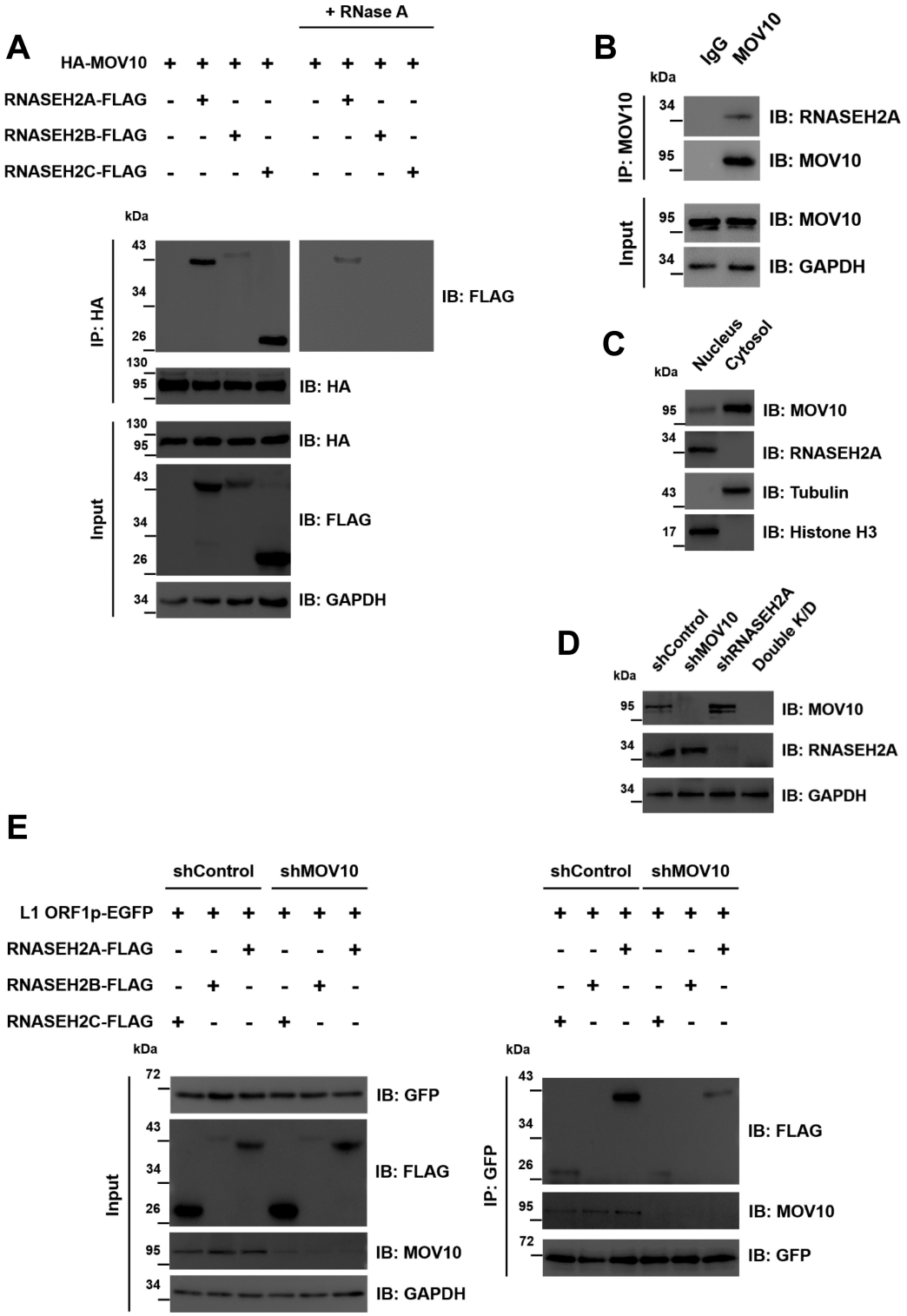

Figure 1. Interaction between RNASEH2 and MOV10 in an RNA-dependent manner. (**A**) Immunoblot analysis of RNASEH2 subunits in both cell lysates and eluates in co-immunoprecipitation experiments. Corresponding expression constructs were co-transfected into HeLa cells. At 48 h post-transfection, the cells were harvested for the co-immunoprecipitation assays. Total cell lysates were treated with or without RNase A prior to the immunoprecipitation procedure. GAPDH served as the loading control, and molecular weight standards are indicated in kDa. (**B**) Immunoblot analysis of endogenous MOV10 and RNASEH2A followed by co-immunoprecipitation with either anti-IgG or anti-MOV10 antibody. (**C**) Immunoblot analysis results showing levels of endogenous MOV10 and RNASEH2A in nuclear and cytosol fractions. (**D**) Western blot analysis of total cell extracts prepared from shRNA-mediated knockdown HeLa cells using anti-MOV10, anti-RNASEH2A and anti-GAPDH antibody. The knockdown efficiency of either endogenous MOV10 or RNASEH2A was confirmed. GAPDH served as the loading control. (**E**) Immunoblot analysis showing levels of RNASEH2 components in either control or MOV10-deficient HeLa cells following co-immunoprecipitation with anti-GFP antibody. GAPDH served as the loading control, and molecular weight standards are indicated in kDa.

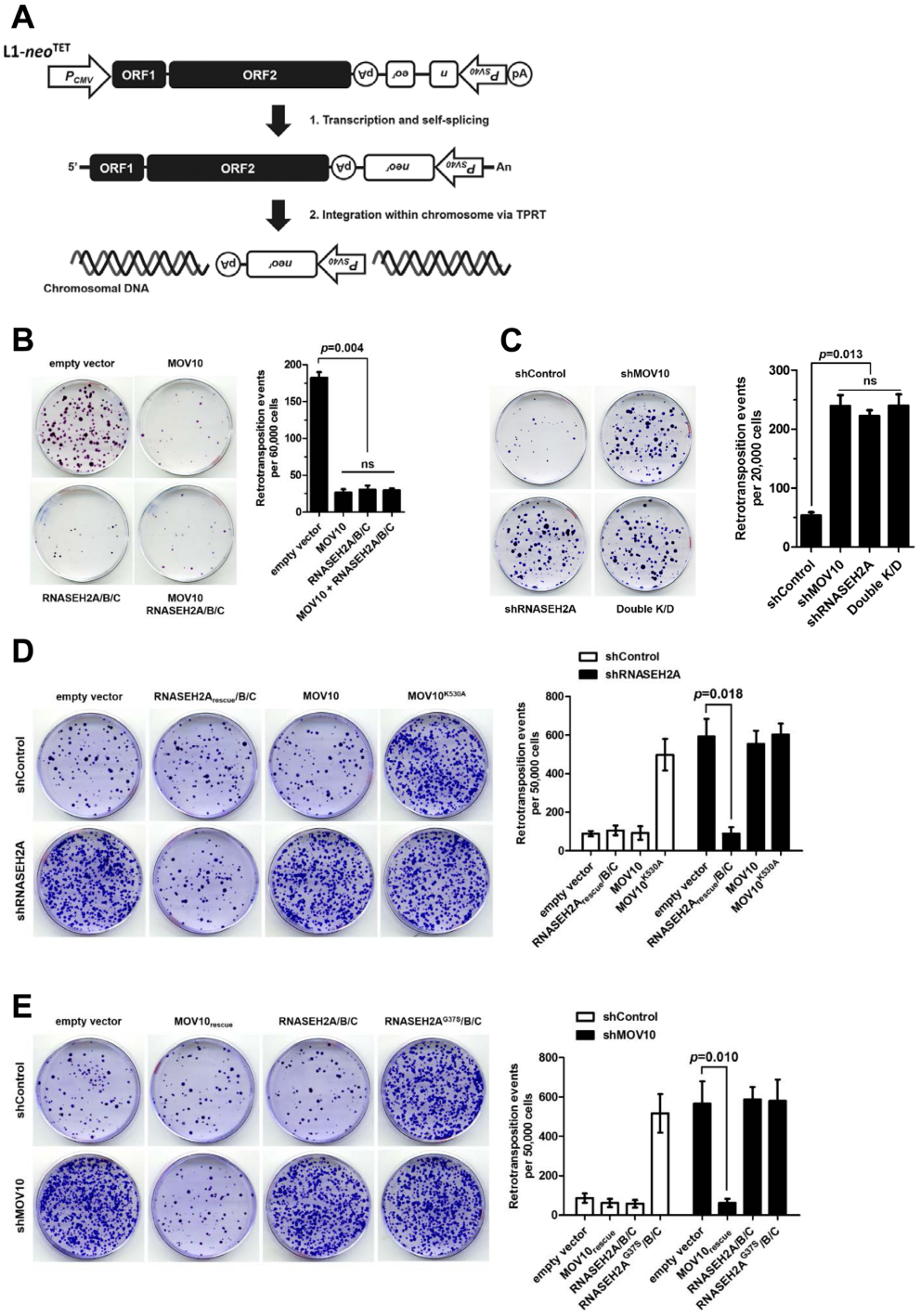

Figure 2. Suppression of L1 mobility by interplay between RNASEH2 and MOV10. (**A**) A schematic drawing of the L1 construct and an overview of the L1 retrotransposition assay. The L1-*neo*^{TET} expression cassette is a complete retrocompetent L1 element that encodes L1 ORF1p and L1 ORF2p driven by a CMV promoter. The L1 construct carries a retrotransposition indicator cassette near its 3′ UTR. The cassette contains the neomycin phosphotransferase gene (*neo*^{r}) interrupted by a tetrahymena self-splicing intron (36) in an anti-sense orientation relative to the transcriptional orientation of the L1 element. The intron is spliced out of the full-length L1 RNA transcript. The spliced L1 RNA is reverse-transcribed, and the resulting cDNA is integrated into the genome. Retrotransposition of the resulting RNA leads to expression of the indicator gene, conferring G418-resistance to host cells. (**B**) L1 assays were carried out following co-transfection of the indicated expression vectors with the L1-*neo*^{TET} expression cassette at a ratio of 1:1 into HeLa cells. The cells were subjected to selection for up to 14 days in the presence of G418 (1 mg/ml). Following G418 selection, G418-resistant foci were stained with crystal violet solution. (**C**) L1 retrotransposition assays using L1-*neo*^{TET} cassette performed in either MOV10- or RNASEH2A-deficient HeLa cells. (**D**) L1 assays performed by co-transfection of L1-*neo*^{TET} expression cassette with the indicated expression vectors at a ratio of 1:1 into RNASEH2A-depleted HeLa cells. (**E**) L1 retrotransposition assays performed in MOV10-depleted HeLa cells by introduction of the indicated expression vectors and the L1-*neo*^{TET} expression cassette at a ratio of 1:1. Representative culture dishes for each condition are shown. The graph represents quantitation of the L1 assays, and the *Y*-axis depicts the number of G418-resistant foci per 20,000 ∼ 60,000 cells, as indicated. Data are shown as the mean ± standard deviation (SD) of a single experiment with three replicates. Statistical significance was determined by two-tailed Student's *t*-test with the *p*-values indicated (ns = not significant).

Consistent with the previous study (13), the number of G418-resistant colonies representing a successful L1 retrotransposition dramatically increased when endogenous MOV10 was depleted by shRNA-mediated knockdown (Figure 1D and 2C). Similarly, knockdown of endogenous RNASEH2A resulted in increased L1 mobility (Figure 1D and 2C). Furthermore, simultaneous depletion of both cellular MOV10 and RNASEH2A resulted in a similar degree of L1 restriction that was achieved by individual knockdown of the genes (Figure 1D and 2C). In agreement with these results, the elevated L1 retrotransposition rate was accompanied by a concomitant increase in spliced L1 DNA levels in MOV10- and RNASEH2A-deficient HeLa cells transfected with the *Fluc*-carrying L1 cassette (pYX017) (Supplementary Figure S2A). To verify the specificity of our knockdown experiments by reconstitution with shRNA-resistant expression vectors (hereafter referred to as $MOV10_{rescue}$ or $RNASEH2A_{rescue}$), the shRNA-resistant MOV10 ($MOV10_{rescue}$) was co-transfected with L1-neo^{TET} into HeLa cells transduced with shRNA targeting *MOV10* mRNA or a control (Supplementary Figure S2B). The expression of $MOV10_{rescue}$ markedly decreased the number of G418-resistant cells, suggesting that the observed increase of L1 retrotransposition upon knockdown of MOV10 likely reflects an on-target rather than off-target effect of the MOV10 shRNA (Figure 2E). Similarly, the shRNA-mediated RNASEH2A knockdown phenotype was rescued by ectopic expression of the shRNA-resistant RNASEH2A ($RNASEH2A_{rescue}$) in combination with RNASEH2B and C subunits (Figure 2D and Supplementary Figure S2C).

Because RNASEH2 interacts with MOV10 in an RNA-dependent manner and restricts L1 retrotransposition, we thus hypothesized that RNASEH2 may function together with MOV10 to prevent L1 mobility. To address this hypothesis, we transiently co-transfected the L1 expression cassette with the MOV10 expression vector into RNASEH2A-deficient HeLa cells. Ectopically expressed MOV10, despite its potent anti-retroelement activity, failed to restrict L1 retrotransposition (Figure 2D) in RNASEH2A-depleted cells. Instead, the retrotransposition efficiency was similar to that in helicase-defective $MOV10^{K530A}$-expressing cells (Figure 2D). Given the role of RNA helicase activity in MOV10-mediated L1 control, overexpression of $MOV10^{K530A}$ served as a negative control. Conversely, overexpression of RNASEH2 in cellular MOV10-deficient cells did not affect L1 replication despite its ability to inhibit L1 mobility (Figure 2C and 2E), indicating that RNASEH2 is a negative regulator of L1 function in a MOV10-dependent manner. The functionally defective RNASEH2 (30) found in AGS patient ($RNASEH2A^{G37S}$) was included as a negative control. We thus concluded that the interplay between RNASEH2 and MOV10 is crucial for controlling L1 retrotransposition.

RNASEH2 associates with L1-derived RNAs in a MOV10-dependent manner

To determine if both RNASEH2 and MOV10 associate with L1-derived RNAs, especially in the nucleus, we transiently co-transfected pAD3TE1 with RNASEH2 components and MOV10 into HeLa cells. The pAD3TE1 plasmid contains the MS2 stem loop structures in the L1 3′ UTR (38). Thus, we employed this expression cassette to visualize the asymmetric distribution and trafficking of *de novo*, intercellular L1-derived RNAs. When RNASEH2 components were co-expressed with MS2 stem loops-containing L1 RNAs, both RNASEH2A and L1-derived RNAs were co-localized in the nucleus (Figure 3A, upper panel). Given that human RNASEH2 originally assembles in the cytoplasm and translocates to the nucleus in an RNASEH2B-dependent manner (45), the co-localization in the nucleus may confer its enzymatic function. MOV10 was similarly present with L1-derived RNAs in cytoplasmic foci as well as in the nuclei of transfected cells indicated by the white arrow (Figure 3A, middle panel). Of note, we observed nuclear co-localization of RNASEH2A and MOV10 in L1-expressing HeLa cells (Figure 3A, lower panel), indicating that both RNASEH2 and MOV10 can associate with L1-derived RNAs in the nucleus.

To further substantiate this conclusion, we next examined the association of individual proteins and spliced L1-specific RNAs using RNA immunoprecipitation assays. These results revealed a significant abundance of L1-derived RNAs in immunoprecipitates from MOV10-expressing cells when compared with control cells (Figure 3B), suggesting that MOV10 associates with *de novo* L1 RNAs. Similarly, co-precipitated L1-derived RNAs were highly enriched in RNASEH2A immunoprecipitates, whereas the signal was diminished in the control immunoprecipitation samples where cells were transfected with empty vectors. These results suggest an association between RNASEH2A and spliced L1-specific RNAs (Figure 3C). Notably, the fold change was more pronounced in cells co-expressing RNASEH2A and MOV10, with an ∼7-fold increase (Figure 3C). These results demonstrate an association between RNASEH2A and spliced L1-derived RNAs in a MOV10-dependent manner. In contrast, depletion of endogenous MOV10 resulted in a significant decrease in *de novo* L1 RNA abundance (Figure 3D). Taken together, these data support the conclusion that RNASEH2 interacts with *de novo* L1 RNAs in a MOV10-dependent manner.

Loss of MOV10 results in an accumulation of L1-derived RNA-DNA hybrids

Impairment of RNA-DNA hybrid resolution has been suggested to be associated with genomic instability and an accumulation of L1 DNAs in AGS patient-derived fibroblasts (32). Using S9.6 antibody that specifically recognizes the intermediate A/B helical RNA-DNA duplex conformation (46), we explored whether deficiency of MOV10 would result in accumulation of RNA-DNA hybrids.

A nuclear enrichment of the S9.6-positive foci was observed in stably RNASEH2A-depleted cells (Figure 4A, white arrowheads). The few cytoplasmic signals may be due to mitochondrial DNA replication (47) or unusual RNA conformations (48). Intriguingly, shRNA-mediated depletion of MOV10 also led to an accumulation of the S9.6-positive nucleolar localization signals in the nucleus (Figure 4A, white arrowheads), suggesting that endogenous MOV10 prevents formation of RNA-DNA hybrids. In con-

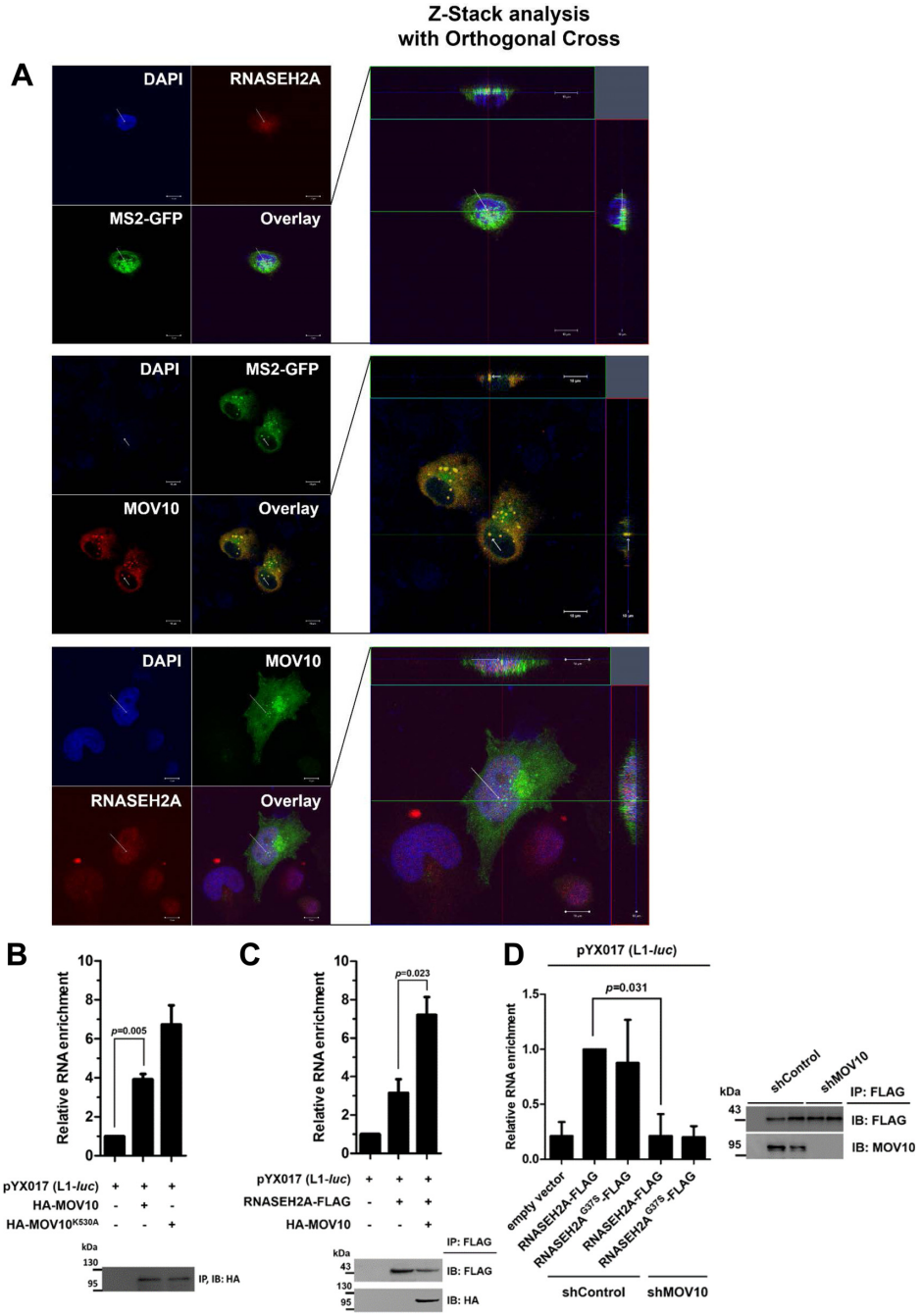

Figure 3. Association of RNASEH2 with L1 RNAs in MOV10-dependent manner. (**A**) Immunofluorescent confocal microscopy (including Z-stacks) showing the subcellular distribution of L1-derived RNAs, MOV10 and RNASEH2A. HeLa cells were transfected with pAD3TE1, a plasmid expressing a nuclear localized MS2-GFP fusion protein. These microscopy results revealed L1 RNA accumulation in both cytoplasmic and nuclear foci by exploiting the 24 MS2-binding sites in the pAD3TE1-derived L1 RNA. For detection of MOV10 and RNASEH2A, either anti-MOV10 antibody or anti-RNASEH2A antibody was used as a primary antibody, respectively. Green and red lines indicate corresponding points in the orthogonal planes, showing localization of the label within the pictured cell. The scale bar represents 10 μm. (**B**) RNA immunoprecipitation carried out in HeLa cells co-transfected with either N-terminally HA-tagged MOV10 or N-terminally HA-tagged MOV10^{K530A} and the L1-*luc* cassette (pYX017). At 48 h post-transfection, whole cell extracts were subjected to RNA immunoprecipitation using anti-HA antibody. The RT-qPCR was carried out using primers specific to spliced *Fluc* cassette. The relative abundances of the immunoprecipitated RNA are represented as fold change over the input, relative to *RN7SL1* levels. (**C**) RNA immunoprecipitation performed in HeLa cells co-expressing the indicated combinations of expression plasmids with pYX017. The anti-FLAG antibody was used for RNA immunoprecipitation, and the resulting RNAs in the immunoprecipitates were quantified by RT-qPCR using primers specific to spliced *Fluc* cassette. The relative abundances of the immunoprecipitated RNA are represented as fold change over the input, relative to *RN7SL1* levels. (**D**) RNA immunoprecipitation performed in HeLa cells co-transfected with C-terminally FLAG-tagged RNASEH2A or C-terminally FLAG-tagged RNASEH2A^{G37S} with pYX017. Cell extracts were subjected to immunoprecipitation using anti-FLAG antibody. The resulting RNAs were subjected to RT-qPCR using primers specific to spliced *Fluc* cassette. The relative occupancy of the resulting immunoprecipitated RNAs is represented as fold change over the input material, relative to *RN7SL1* levels. Data are presented as the mean ± SD of three independent experiments. Statistical significance was determined using the two-tailed Student's *t*-test with the *p*-values indicated.

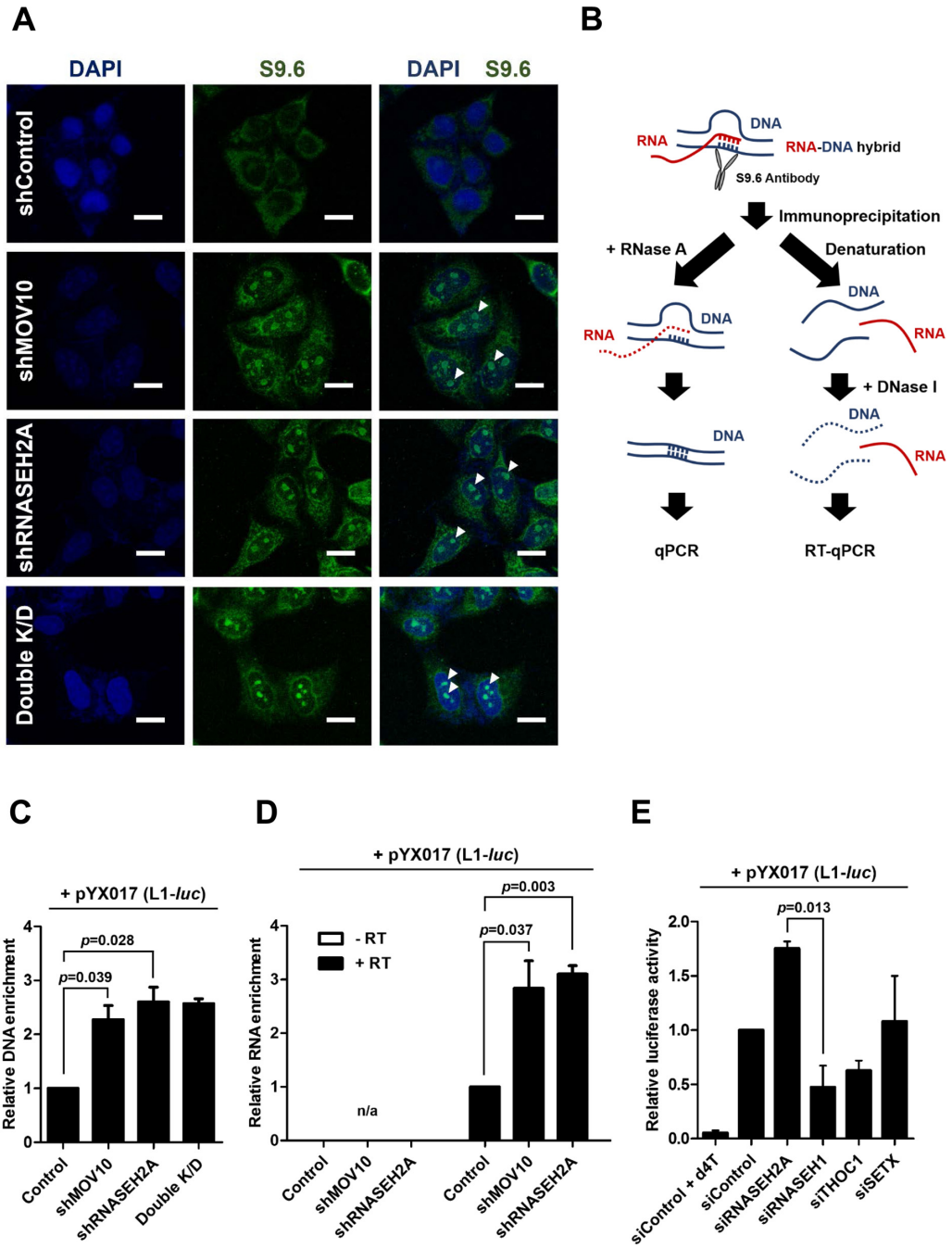

Figure 4. Accumulation of L1-derived RNA-DNA hybrids in MOV10- and RNASEH2A-deficient cells. (**A**) Immunofluorescence analysis of RNA-DNA hybrids using S9.6 antibody showing the control, MOV10- and RNASEH2A-depleted cells, respectively. A merge of the two channels is shown with the nucleus stained with DAPI. The scale bar represents 10 μm. (**B**) A schematic comparison of DRIP-qPCR and DRIP-RT-qPCR procedure. (**C**) Results of DRIP-qPCR following immunoprecipitation using the S9.6 antibody upon 36 h post-transfection with pYX017 (L1-*luc*). DRIP-qPCR was performed using primers specific to the spliced *Fluc* region in transfected HeLa cells. The relative abundance of RNA-DNA hybrids immunoprecipitated is represented as fold change over the input material. The data were normalized to *MDM2* levels. The data are represented as mean ± SD values from three independent experiments analyzed by two-tailed Student's *t*-test with *p*-values indicated. (**D**) DRIP-RT-qPCR performed in HeLa cells transfected with pYX017 (L1-*luc*). Samples were harvested at 24 h post-transfection and subjected to immunoprecipitation using the S9.6 antibody. The resulting RNAs in the immunoprecipitates were quantified by RT-qPCR using primers specific to spliced *Fluc* cassette. The relative occupancy of immunoprecipitated RNA is represented as fold change over the input material. The data were normalized to *RN7SL1* levels. − RT indicates the negative controls for each sample without reverse transcriptase. Data are presented as the mean ± SD of three independent experiments and were analyzed by two-tailed Student's *t*-test with the *p*-value indicated. (n/a = not available). (**E**) L1 retrotransposition assay using L1-*luc* cassette (pYX017) performed in HeLa cells transfected with corresponding siRNAs. This luciferase reporter-based L1 assay system was previously described (37). A firefly luciferase (*Fluc*) gene, instead of *neo*^{r}, is disrupted by an intronic sequence and inserted in the 3′ UTR of L1 in an anti-sense orientation relative to the L1 genes under the control of an independent promoter. A *Renilla* luciferase (*Rluc*) cassette is inserted in the same backbone to allow the normalization. Luciferase activity was determined as the ratio of Fluc/Rluc. Cells treated with 50 μM stavudine (d4T) served as a negative control. Data are presented as the mean ± SD of three independent experiments and were analyzed with two-tailed Student's *t*-test with the *p*-values indicated.

trast, nucleoplasmic foci were rarely detected in control cells (Figure 4A).

The RNA-DNA hybrids accumulation in either MOV10- or RNASEH2A-deficient cells was also quantitated by HB-GFP retention FACS analysis (40). As HB-GFP interacts with heteroduplexes in the nucleus, it is retained in the nucleus following permeabilization with detergent. This leads to a significant number of GFP-positive cells, whereas cytoplasmic GFP is completely washed out. Similar to the intense staining in the nucleolar region with the S9.6 antibody (Figure 4A), depletion of either MOV10 or RNASEH2A increased the number of GFP-positive cells (Supplementary Figure S3A).

L1-derived RNA-DNA hybrids are produced as vital intermediates during L1 TPRT (3). To investigate whether RNASEH2 and MOV10 prevent formation of L1-derived heteroduplexes, we quantitated either L1-derived DNAs or RNAs following RNA-DNA hybrid immunoprecipitation (hereafter referred to as DRIP-qPCR) (Figure 4B). Results from DRIP-qPCR using primers specific to spliced *Fluc* cassette revealed an accumulation of L1-derived heteroduplexes in both RNASEH2A- and MOV10-deficient cells (Figure 4C). This was concomitant with an increase in HB-GFP retention by ectopic introduction of the L1-*neo*^{TET} expression cassette into either RNASEH2A- or MOV10-depleted cells (Supplementary Figure S3B). Cells transfected with the L1 expression cassette (pYX017) exhibited a significant change in abundance of *de novo* L1-specific RNAs (Figure 4D), demonstrating that both RNASEH2 and MOV10 are involved in resolving heteroduplex intermediates during L1 retrotransposition.

We then sought to determine whether other proteins involved in resolution of cellular RNA-DNA hybrids contribute to L1 control. To examine this, we transiently knocked-down a panel of cellular R-loop suppressors (49), especially RNASEH1, THO complex subunit 1 (THOC1) and a probable helicase senataxin (SETX) and performed dual luciferase-based L1 retrotransposition assays. Most of the R-loop suppressors did not affect L1 control (Figure 4E, Supplementary Figure S3C and S3D). Intriguingly, human RNASEH1 did not exert any inhibitory effects on L1 suppression despite its RNase H activity, suggesting that RNASEH2 specifically recognizes L1-derived RNA-DNA intermediates (Figure 4E). Overall, these results indicate that RNASEH2, together with MOV10, specifically contribute to prevention of L1 heteroduplex formation during L1 retrotransposition.

Interaction of MOV10 with L1 ORF1p and MOV10 helicase activity are required for RNASEH2-mediated L1 restriction

RNA helicase activity of MOV10 has been implicated as a crucial modulator of L1 mobility (15). Thus, we hypothesized that the putative helicase domain is necessary for the anti-L1 activity of MOV10. To analyze the functions of the MOV10 domains, we constructed two truncated MOV10 variants, N-terminal MOV10 and C-terminal MOV10 (Figure 5A). Since the N-terminal domain of MOV10 is required for its interaction with the HIV-1 nucleocapsid protein (12), we first determined if MOV10 interacts with L1 ORF1p via its N-terminal domain. As shown in Figure 5B, the full-length MOV10 strongly interacted with L1 ORF1p and the N-terminal MOV10 also associated with L1 ORF1p. However, no interaction was observed with the C-terminal MOV10 (Figure 5B), indicating that the N-terminal portion of MOV10 is required for its association with L1 ORF1p.

Next, we tested interactions between the truncated MOV10 variants and RNASEH2. Similar to their interactions with L1 ORF1p, the N-terminal region of MOV10 was sufficient to interact with the catalytic subunit of RNASEH2A (Figure 5C). However, only the full-length MOV10 was able to interact with the auxiliary subunits of RNASEH2 (Figure 5D and 5E), demonstrating that full-length MOV10 is crucial for a functional interaction to occur with both L1 ORF1p and RNASEH2. Consistent with this, ectopic expression of the N-terminal portion of MOV10 lacking the RNA helicase domain completely abolished its anti-L1 activity (Figure 5A). Overexpression of either the C-terminal portion of MOV10 or the helicase-defective MOV10 variant (MOV10^{K530A}) also failed to control L1 mobility (Figure 5A). Taken together, these results indicate that MOV10 mediates a functional association with both L1 ORF1p and RNASEH2, and its RNA helicase activity is required for the RNASEH2-mediated L1 suppression.

RNASEH2-MOV10-mediated L1 restriction is linked to rheumatoid arthritis progression

To gain insight into the biological implications of L1 suppression, we sought to examine whether RNASEH2-MOV10-mediated L1 regulation affects the progression of L1-derived autoimmune diseases, such as rheumatoid arthritis (RA). To test this, we performed the *neo*^{r} indicator-based L1 assays using the human synovial sarcoma cell line, SW982, which is known to express inflammatory cytokines and MMPs in response to IL-1β (50). Overexpression of MOV10 led to a significant decrease in L1 mobility in SW982 cells; however, helicase-defective MOV10^{K530A} lost its ability to negatively control L1 retrotransposition (Figure 6A). Introduction of RNASEH2 also impaired the formation of G418-resistant foci to similar level in MOV10-expressing cells. In contrast, the functionally defective RNASEH2A^{G37S} failed to prevent L1 retrotransposition, indicating that RNASEH2 activity is required for L1 restriction. Furthermore, the anti-L1 activity was markedly attenuated when RNASEH2A^{G37S} was co-expressed with MOV10, suggesting that the interplay between MOV10 and RNASEH2 is essential for inhibition of L1 retrotransposition (Figure 6A).

We next tested whether the RNASEH2-MOV10-mediated L1 restriction would prevent activation of synovial cells. To test the hypothesis, we measured IL-6 and TNF-α levels in culture media of cells used in L1 assays. L1 activation led to significantly elevated levels of both IL-6 (Figure 6B) and TNF-α (Figure 6C) in SW982 cells, while secretion of these cytokines was markedly diminished by RNASEH2-MOV10-mediated L1 restriction. However, co-expression of MOV10 with an enzymatically inactive form of RNASEH2A did not inhibit L1 activity, thereby increasing IL-6 (Figure 6B) and TNF-α production

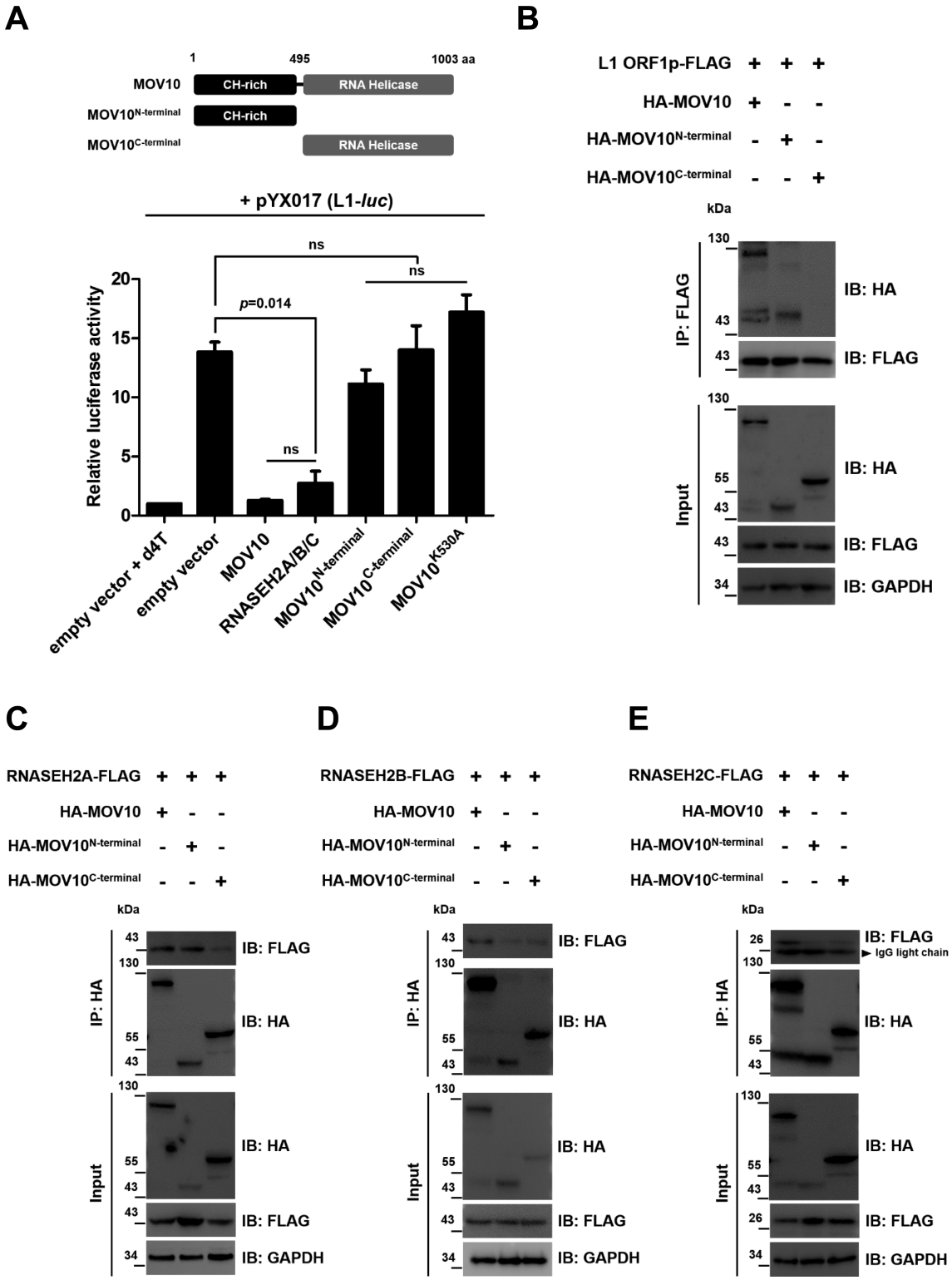

Figure 5. Contribution of MOV10 as an interaction mediator between L1 ORF1p and RNASEH2 for L1 suppression. (**A**) (Upper panel) A schematic drawing of MOV10 variants. (Lower panel) L1 retrotransposition assays using L1-*luc* cassette performed in HeLa cells co-transfected with corresponding MOV10 variants and pYX017 at a ratio of 1:1. Treatment of d4T (50 μM) served as a negative control. Data are presented as the mean ± SD of three independent experiments and were analyzed with two-tailed Student's *t*-test with the *p*-values indicated. (**B**) Immunoblot results showing the levels of MOV10 variants in both cell lysates and eluates followed by co-immunoprecipitation. Both L1 ORF1p expression vector and the corresponding MOV10 variants were co-transfected into HeLa cells. At 48 h post-transfection, the cells were harvested for co-immunoprecipitation assays using anti-FLAG antibody. (**C**–**E**) Western blot analyses showing levels of RNASEH2 components in HeLa cells co-transfected with indicated combinations of expression plasmids following co-immunoprecipitation with anti-HA antibody. GAPDH served as the loading control, and molecular weight standards are indicated in kDa.

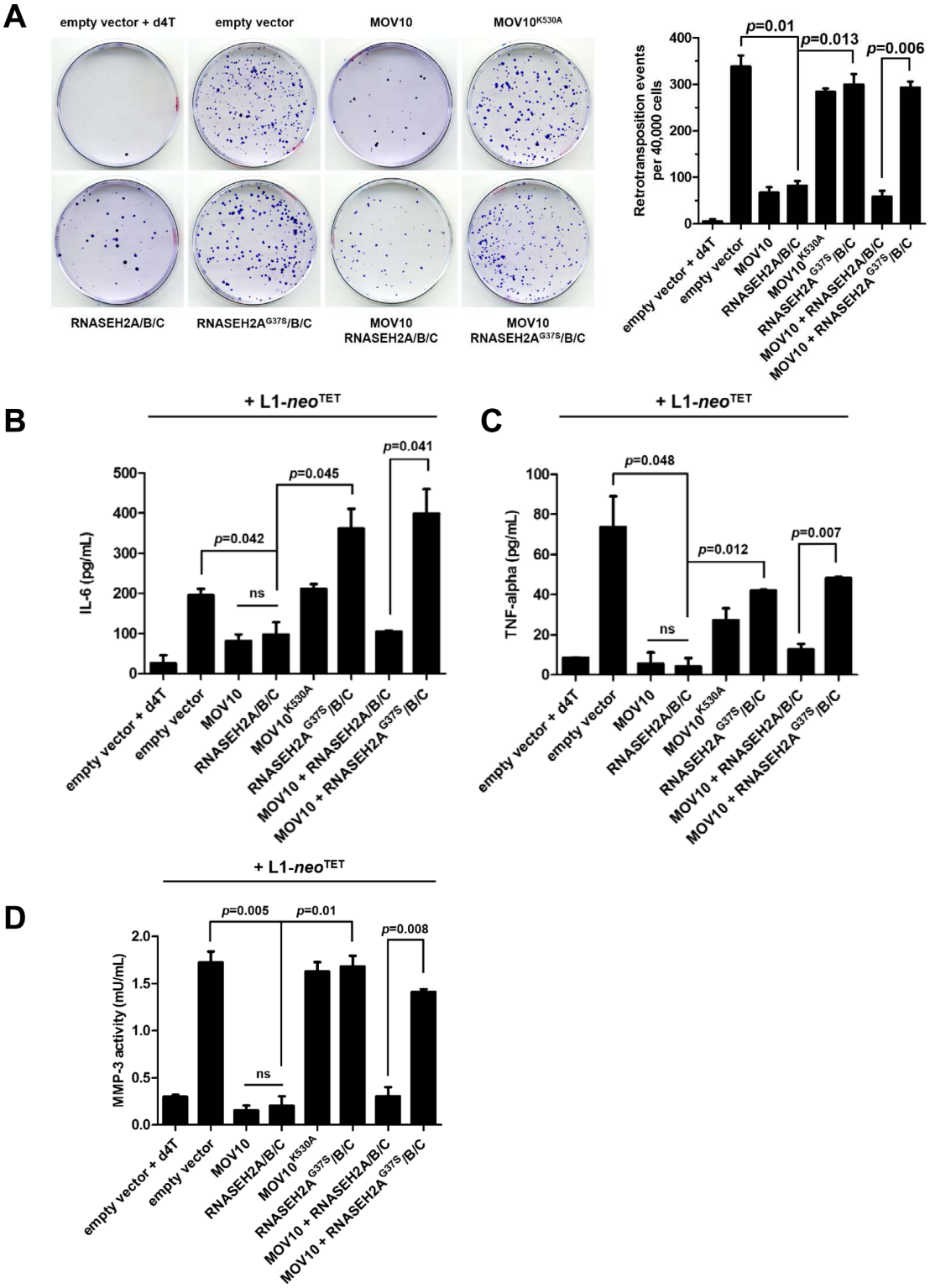

Figure 6. A causal relationship between L1 restriction and RA-related gene expressions. (**A**) L1 retrotransposition assays using L1-*neo*^{TET} cassette performed in synovial SW982 cells co-transfected with corresponding expression vectors and the L1-*neo*^{TET} expression cassette at a ratio of 1:1. The transfected cells were subjected to selection for 10 ∼ 12 days with G418 (1 mg/ml). Following selection, G418-resistant foci were stained with crystal violet solution. Representative culture dishes for each condition are shown. Quantitation of the L1 assays was plotted. The *Y*-axis depicts the number of G418-resistant foci per 40,000 cells. Data are shown as the mean ± SD from an experiment with three replicates and were analyzed by two-tailed Student's *t*-test with the *p*-values indicated. (**B**–**D**) Levels of inflammatory cytokines and MMP-3 activity. In parallel to L1 assay shown in (A), cell culture supernatants were harvested at 72 h post-transfection and analyzed by enzyme-linked immunosorbent assay (ELISA) to detect (B) IL-6 and (C) TNF-α levels in SW982 cells, and fluorometric immunocapture assays were performed to detect (D) MMP-3 activity. Data are presented as the mean ± SD of three independent experiments, and statistical significance was determined using the two-tailed Student's *t*-test with the *p*-values indicated.

(Figure 6C). These data demonstrated that the RNASEH2-MOV10-mediated L1 control is linked to regulation of RA-related cytokine induction.

Activated synovial cells also express matrix-degrading enzymes, a pathological indicator of RA. Thus, the MMP-3 activity in cell culture supernatant was monitored. MMP-3 activity profiles displayed a causal relationship with the RNASEH2-MOV10-mediated L1 suppression (Figure 6D), suggesting a potential causal relationship between L1 suppression and RA-related disease progression.

DISCUSSION

The function of MOV10 to inhibit L1 retrotransposition is conserved across diverse host species (13,15). Early studies showed that MOV10 localizes to cytoplasmic granules. It sequesters L1 RNPs by interacting with L1 ORF1p, thereby facilitating L1 RNA degradation. Later, it was revealed that MOV10 suppresses L1 mobility in the nucleus (17). However, the precise mechanism has not been fully determined. Therefore, the elucidation of MOV10-interacting networks could contribute to a better understanding of the cellular functions of MOV10, particularly how MOV10 controls L1 mobility.

In the present study, we identified a novel interaction partner of MOV10, the host protein complex RNASEH2. RNASEH2 associates with L1-derived RNAs in a MOV10-dependent manner, and the interplay between RNASEH2 and MOV10 is crucial for L1 suppression. Furthermore, we have shown that the RNASEH2-MOV10-mediated L1 control inhibits expression of RA-related indicators in synovial cells, which provided evidence of its physiological relevance. Our results have identified a previously unknown mechanism by which both RNASEH2 and MOV10 specifically interfere a formation of L1-drived RNA-DNA hybrids during L1 retrotransposition in the nucleus (Supplementary Figure S4).

Extrapolating from a study on MOV10-mediated retroviral restriction (51), MOV10 may enhance RNASEH2 activity during L1 retrotransposition by either changing L1 RNA secondary structures or through steric hindrance. In support of this hypothesis, the helicase-defective form of MOV10 was unable to restrict L1 mobility (Figure 5A). It is also plausible that the 5′ to 3′ unwinding activity of MOV10 causes steric hindrances during L1 ORF2p-dependent reverse transcription. Even though an interaction between MOV10 and L1 ORF2p was not observed in our experiments (Supplementary Figure S1B), this possibility cannot be ruled out. There may be an additive or even a synergistic benefit for the RNASEH2-mediated resolution of L1 hybrid intermediates during L1 retrotransposition.

Remarkably, depletion of either RNASEH2A or MOV10 leads to an increase in L1-specific RNA-DNA hybrids, in agreement with a previous study (32). During TPRT, L1 ORF2p binds to the polyA tract of L1 RNA to bring the RNA template to the insertion site (52) where it nicks the genomic DNA to initiate reverse transcription in the 3′ to 5′ direction. Consistent with this, L1-specific signals were predominantly detected at the L1 3′ UTR (Figure 4C and 4D). The predominance of 3′ UTR signal is most likely due to 5′ truncations of L1 during retrotransposition (3). The complexity of L1 RNA structures may have also influenced the DRIP-based qPCR results, because RNA-DNA hybrids are often present at UTRs of genes that post-transcriptionally control gene expressions (42).

In addition to RNASEH2, RNASEH1 is also capable of catalyzing the cleavage of RNAs via hydrolysis; however, it does not affect L1 restriction (Figure 4E). This suggests that these enzymes might have different substrate specificities. Based on these results, it is possible that RNASEH2 functionality as a L1 restriction factor depends on MOV10, which may enable RNASEH2 to recognize the characteristic heteroduplexes of L1. Therefore, RNASEH2 appears to be the primary enzyme that specifically regulates a formation of L1-derived RNA-DNA hybrids.

Since a potential role of retroelements as immunogenic sources in autoimmune diseases has been a major interest over the past decades (8), understanding the interplay between RNASEH2 and MOV10 in the impairment of L1 retrotransposition will expand the spectrum of their anti-L1 activity beyond the certain disease regulation. Such insights may improve our understanding of RNASEH2-MOV10-mediated nucleic acid pathways in the context of innate immunity.

SUPPLEMENTARY DATA

Supplementary data are available at NAR Online.

ACKNOWLEDGEMENTS

We are grateful to Dr. Seok-Hyung Kim for providing SW982 cells. 2′,3′-didehydro-2′,3′-dideoxythymidine (d4T; Stavudine) were obtained through the National Institutes of Health AIDS Reagent Program (Division of AIDS, NIAID, NIH).

FUNDING

Samsung Science and Technology Foundation [SSTF-BA1402–19]. Funding for open access charge: Samsung Science and Technology Foundation [SSTF-BA1402-19].
Conflict of interest statement. None declared.

REFERENCES

1. Lander,E.S., Linton,L.M., Birren,B., Nusbaum,C., Zody,M.C., Baldwin,J., Devon,K., Dewar,K., Doyle,M., FitzHugh,W. *et al.* (2001) Initial sequencing and analysis of the human genome. *Nature*, **409**, 860–921.
2. Luan,D.D., Korman,M.H., Jakubczak,J.L. and Eickbush,T.H. (1993) Reverse transcription of R2Bm RNA is primed by a nick at the chromosomal target site: a mechanism for non-LTR retrotransposition. *Cell*, **72**, 595–605.
3. Moran,J.V., Holmes,S.E., Naas,T.P., DeBerardinis,R.J., Boeke,J.D. and Kazazian,H.H. Jr (1996) High frequency retrotransposition in cultured mammalian cells. *Cell*, **87**, 917–927.
4. Hancks,D.C. and Kazazian,H.H. Jr (2012) Active human retrotransposons: variation and disease. *Curr. Opin. Genet. Dev.*, **22**, 191–203.
5. Miki,Y., Nishisho,I., Horii,A., Miyoshi,Y., Utsunomiya,J., Kinzler,K.W., Vogelstein,B. and Nakamura,Y. (1992) Disruption of the APC gene by a retrotransposal insertion of L1 sequence in a colon cancer. *Cancer Res.*, **52**, 643–645.
6. Kazazian,H.H. Jr and Moran,J.V. (1998) The impact of L1 retrotransposons on the human genome. *Nat. Genet.*, **19**, 19–24.

7. Gasior,S.L., Wakeman,T.P., Xu,B. and Deininger,P.L. (2006) The human LINE-1 retrotransposon creates DNA double-strand breaks. *J. Mol. Biol.*, **357**, 1383–1393.
8. Volkman,H.E. and Stetson,D.B. (2014) The enemy within: endogenous retroelements and autoimmune disease. *Nat. Immunol.*, **15**, 415–422.
9. Hamann,L., Jensen,K. and Harbers,K. (1993) Consecutive inactivation of both alleles of the gb110 gene has no effect on the proliferation and differentiation of mouse embryonic stem cells. *Gene*, **126**, 279–284.
10. Gregersen,L.H., Schueler,M., Munschauer,M., Mastrobuoni,G., Chen,W., Kempa,S., Dieterich,C. and Landthaler,M. (2014) MOV10 Is a 5′ to 3′ RNA helicase contributing to UPF1 mRNA target degradation by translocation along 3′ UTRs. *Mol. Cell*, **54**, 573–585.
11. Burdick,R., Smith,J.L., Chaipan,C., Friew,Y., Chen,J., Venkatachari,N.J., Delviks-Frankenberry,K.A., Hu,W.S. and Pathak,V.K. (2010) P body-associated protein Mov10 inhibits HIV-1 replication at multiple stages. *J. Virol.*, **84**, 10241–10253.
12. Wang,X., Han,Y., Dang,Y., Fu,W., Zhou,T., Ptak,R.G. and Zheng,Y.H. (2010) Moloney leukemia virus 10 (MOV10) protein inhibits retrovirus replication. *J. Biol. Chem.*, **285**, 14346–14355.
13. Arjan-Odedra,S., Swanson,C.M., Sherer,N.M., Wolinsky,S.M. and Malim,M.H. (2012) Endogenous MOV10 inhibits the retrotransposition of endogenous retroelements but not the replication of exogenous retroviruses. *Retrovirology*, **9**, 53.
14. Goodier,J.L., Cheung,L.E. and Kazazian,H.H. Jr (2012) MOV10 RNA helicase is a potent inhibitor of retrotransposition in cells. *PLoS Genet.*, **8**, e1002941.
15. Li,X., Zhang,J., Jia,R., Cheng,V., Xu,X., Qiao,W., Guo,F., Liang,C. and Cen,S. (2013) The MOV10 helicase inhibits LINE-1 mobility. *J. Biol. Chem.*, **288**, 21148–21160.
16. Moldovan,J.B. and Moran,J.V. (2015) The zinc-finger antiviral protein ZAP inhibits LINE and alu retrotransposition. *PLoS Genet.*, **11**, e1005121.
17. Skariah,G., Seimetz,J., Norsworthy,M., Lannom,M.C., Kenny,P.J., Elrakhawy,M., Forsthoefel,C., Drnevich,J., Kalsotra,A. and Ceman,S. (2017) Mov10 suppresses retroelements and regulates neuronal development and function in the developing brain. *BMC Biol.*, **15**, 54.
18. Malik,H.S. and Eickbush,T.H. (2001) Phylogenetic analysis of ribonuclease H domains suggests a late, chimeric origin of LTR retrotransposable elements and retroviruses. *Genome Res.*, **11**, 1187–1197.
19. Malik,H.S., Henikoff,S. and Eickbush,T.H. (2000) Poised for contagion: evolutionary origins of the infectious abilities of invertebrate retroviruses. *Genome Res.*, **10**, 1307–1318.
20. Kenny,P.J., Zhou,H., Kim,M., Skariah,G., Khetani,R.S., Drnevich,J., Arcila,M.L., Kosik,K.S. and Ceman,S. (2014) MOV10 and FMRP regulate AGO2 association with microRNA recognition elements. *Cell Rep.*, **9**, 1729–1741.
21. Furtak,V., Mulky,A., Rawlings,S.A., Kozhaya,L., Lee,K., Kewalramani,V.N. and Unutmaz,D. (2010) Perturbation of the P-body component Mov10 inhibits HIV-1 infectivity. *PLoS One*, **5**, e9081.
22. El Messaoudi-Aubert,S., Nicholls,J., Maertens,G.N., Brookes,S., Bernstein,E. and Peters,G. (2010) Role for the MOV10 RNA helicase in polycomb-mediated repression of the INK4a tumor suppressor. *Nat. Struct. Mol. Biol.*, **17**, 862–868.
23. Jeong,H.S., Backlund,P.S., Chen,H.C., Karavanov,A.A. and Crouch,R.J. (2004) RNase H2 of Saccharomyces cerevisiae is a complex of three proteins. *Nucleic Acids Res.*, **32**, 407–414.
24. Rychlik,M.P., Chon,H., Cerritelli,S.M., Klimek,P., Crouch,R.J. and Nowotny,M. (2010) Crystal structures of RNase H2 in complex with nucleic acid reveal the mechanism of RNA-DNA junction recognition and cleavage. *Mol. Cell*, **40**, 658–670.
25. Sparks,J.L., Chon,H., Cerritelli,S.M., Kunkel,T.A., Johansson,E., Crouch,R.J. and Burgers,P.M. (2012) RNase H2-initiated ribonucleotide excision repair. *Mol. Cell*, **47**, 980–986.
26. Chon,H., Sparks,J.L., Rychlik,M., Nowotny,M., Burgers,P.M., Crouch,R.J. and Cerritelli,S.M. (2013) RNase H2 roles in genome integrity revealed by unlinking its activities. *Nucleic Acids Res.*, **41**, 3130–3143.
27. Genovesio,A., Kwon,Y.J., Windisch,M.P., Kim,N.Y., Choi,S.Y., Kim,H.C., Jung,S., Mammano,F., Perrin,V., Boese,A.S. *et al.* (2011) Automated genome-wide visual profiling of cellular proteins involved in HIV infection. *J. Biomol. Screen*, **16**, 945–958.
28. Kennedy,E.M., Gavegnano,C., Nguyen,L., Slater,R., Lucas,A., Fromentin,E., Schinazi,R.F. and Kim,B. (2010) Ribonucleoside triphosphates as substrate of human immunodeficiency virus type 1 reverse transcriptase in human macrophages. *J. Biol. Chem.*, **285**, 39380–39391.
29. Ayinde,D., Casartelli,N. and Schwartz,O. (2012) Restricting HIV the SAMHD1 way: through nucleotide starvation. *Nat. Rev. Microbiol.*, **10**, 675–680.
30. Crow,Y.J., Leitch,A., Hayward,B.E., Garner,A., Parmar,R., Griffith,E., Ali,M., Semple,C., Aicardi,J., Babul-Hirji,R. *et al.* (2006) Mutations in genes encoding ribonuclease H2 subunits cause Aicardi-Goutieres syndrome and mimic congenital viral brain infection. *Nat. Genet.*, **38**, 910–916.
31. Perrino,F.W., Harvey,S., Shaban,N.M. and Hollis,T. (2009) RNaseH2 mutants that cause Aicardi-Goutieres syndrome are active nucleases. *J. Mol. Med. (Berl)*, **87**, 25–30.
32. Lim,Y.W., Sanz,L.A., Xu,X., Hartono,S.R. and Chedin,F. (2015) Genome-wide DNA hypomethylation and RNA:DNA hybrid accumulation in Aicardi-Goutieres syndrome. *Elife*, **4**, e08007.
33. Pokatayev,V., Hasin,N., Chon,H., Cerritelli,S.M., Sakhuja,K., Ward,J.M., Morris,H.D., Yan,N. and Crouch,R.J. (2016) RNase H2 catalytic core Aicardi-Goutieres syndrome-related mutant invokes cGAS-STING innate immune-sensing pathway in mice. *J. Exp. Med.*, **213**, 329–336.
34. Bartsch,K., Knittler,K., Borowski,C., Rudnik,S., Damme,M., Aden,K., Spehlmann,M.E., Frey,N., Saftig,P., Chalaris,A. *et al.* (2017) Absence of RNase H2 triggers generation of immunogenic micronuclei removed by autophagy. *Hum. Mol. Genet.*, **26**, 3960–3972.
35. Meister,G., Landthaler,M., Peters,L., Chen,P.Y., Urlaub,H., Luhrmann,R. and Tuschl,T. (2005) Identification of novel argonaute-associated proteins. *Curr. Biol.*, **15**, 2149–2155.
36. Kroutter,E.N., Belancio,V.P., Wagstaff,B.J. and Roy-Engel,A.M. (2009) The RNA polymerase dictates ORF1 requirement and timing of LINE and SINE retrotransposition. *PLoS Genet.*, **5**, e1000458.
37. Xie,Y., Rosser,J.M., Thompson,T.L., Boeke,J.D. and An,W. (2011) Characterization of L1 retrotransposition with high-throughput dual-luciferase assays. *Nucleic Acids Res.*, **39**, e16.
38. Doucet,A.J., Hulme,A.E., Sahinovic,E., Kulpa,D.A., Moldovan,J.B., Kopera,H.C., Athanikar,J.N., Hasnaoui,M., Bucheton,A., Moran,J.V. *et al.* (2010) Characterization of LINE-1 ribonucleoprotein particles. *PLoS Genet.*, **6**, e1001150
39. Fusco,D., Accornero,N., Lavoie,B., Shenoy,S.M., Blanchard,J.M., Singer,R.H. and Bertrand,E. (2003) Single mRNA molecules demonstrate probabilistic movement in living mammalian cells. *Curr. Biol.*, **13**, 161–167.
40. Bhatia,V., Barroso,S.I., Garcia-Rubio,M.L., Tumini,E., Herrera-Moyano,E. and Aguilera,A. (2014) BRCA2 prevents R-loop accumulation and associates with TREX-2 mRNA export factor PCID2. *Nature*, **511**, 362–365.
41. Geissmann,Q. (2013) OpenCFU, a new free and open-source software to count cell colonies and other circular objects. *PLoS One*, **8**, e54072.
42. Ginno,P.A., Lott,P.L., Christensen,H.C., Korf,I. and Chedin,F. (2012) R-loop formation is a distinctive characteristic of unmethylated human CpG island promoters. *Mol. Cell*, **45**, 814–825.
43. Taylor,M.S., LaCava,J., Mita,P., Molloy,K.R., Huang,C.R., Li,D., Adney,E.M., Jiang,H., Burns,K.H., Chait,B.T. *et al.* (2013) Affinity proteomics reveals human host factors implicated in discrete stages of LINE-1 retrotransposition. *Cell*, **155**, 1034–1048.
44. Goodier,J.L., Cheung,L.E. and Kazazian,H.H. Jr (2013) Mapping the LINE1 ORF1 protein interactome reveals associated inhibitors of human retrotransposition. *Nucleic Acids Res.*, **41**, 7401–7419.
45. Kind,B., Muster,B., Staroske,W., Herce,H.D., Sachse,R., Rapp,A., Schmidt,F., Koss,S., Cardoso,M.C. and Lee-Kirsch,M.A. (2014) Altered spatio-temporal dynamics of RNase H2 complex assembly at replication and repair sites in Aicardi-Goutieres syndrome. *Hum. Mol. Genet.*, **23**, 5950–5960.
46. Boguslawski,S.J., Smith,D.E., Michalak,M.A., Mickelson,K.E., Yehle,C.O., Patterson,W.L. and Carrico,R.J. (1986) Characterization of monoclonal antibody to DNA.RNA and its application to immunodetection of hybrids. *J. Immunol. Methods*, **89**, 123–130.

47. Brown,T.A., Tkachuk,A.N. and Clayton,D.A. (2008) Native R-loops persist throughout the mouse mitochondrial DNA genome. *J. Biol. Chem.*, **283**, 36743–36751.
48. Zhang,Z.Z., Pannunzio,N.R., Hsieh,C.L., Yu,K. and Lieber,M.R. (2015) Complexities due to single-stranded RNA during antibody detection of genomic rna:dna hybrids. *BMC Res. Notes*, **8**, 127.
49. Santos-Pereira,J.M. and Aguilera,A. (2015) R loops: new modulators of genome dynamics and function. *Nat. Rev. Genet.*, **16**, 583–597.
50. Yamazaki,T., Yokoyama,T., Akatsu,H., Tukiyama,T. and Tokiwa,T. (2003) Phenotypic characterization of a human synovial sarcoma cell line, SW982, and its response to dexamethasone. *In Vitro Cell Dev. Biol. Anim.*, **39**, 337–339.
51. Lu,C., Luo,Z., Jager,S., Krogan,N.J. and Peterlin,B.M. (2012) Moloney leukemia virus type 10 inhibits reverse transcription and retrotransposition of intracisternal a particles. *J. Virol.*, **86**, 10517–10523.
52. Doucet,A.J., Wilusz,J.E., Miyoshi,T., Liu,Y. and Moran,J.V. (2015) A 3′ Poly(A) tract is required for LINE-1 retrotransposition. *Mol. Cell*, **60**, 728–741.